

PSR J1838–0537: DISCOVERY OF A YOUNG, ENERGETIC GAMMA-RAY PULSAR

H. J. PLETSCHE^{1,2,3}, L. GUILLEMOT^{4,5}, B. ALLEN^{1,6,2}, M. KRAMER^{4,7}, C. AULBERT^{1,2}, H. FEHRMANN^{1,2}, M. G. BARING⁸, F. CAMILO⁹,
P. A. CARAVEO¹⁰, J. E. GROVE¹¹, M. KERR¹², M. MARELLI¹⁰, S. M. RANSOM¹³, P. S. RAY¹¹, AND P. M. SAZ PARKINSON¹⁴

To appear in ApJ Letters

ABSTRACT

We report the discovery of PSR J1838–0537, a gamma-ray pulsar found through a blind search of data from the *Fermi* Large Area Telescope (LAT). The pulsar has a spin frequency of 6.9 Hz and a frequency derivative of -2.2×10^{-11} Hz s⁻¹, implying a young characteristic age of 4970 years and a large spin-down power of 5.9×10^{36} erg s⁻¹. Follow-up observations with radio telescopes detected no pulsations, thus PSR J1838–0537 appears radio-quiet as viewed from Earth. In September 2009 the pulsar suffered the largest glitch so far seen in any gamma-ray-only pulsar, causing a relative increase in spin frequency of about 5.5×10^{-6} . After the glitch, during a putative recovery period, the timing analysis is complicated by the sparsity of the LAT photon data, the weakness of the pulsations, and the reduction in average exposure from a coincidental, contemporaneous change in the LAT’s sky-survey observing pattern. The pulsar’s sky position is coincident with the spatially extended TeV source HESS J1841–055 detected by the High Energy Stereoscopic System (H.E.S.S.). The inferred energetics suggest that HESS J1841–055 contains a pulsar wind nebula powered by the pulsar.

Subject headings: gamma rays: stars – pulsars: individual (PSR J1838–0537) – ISM: individual objects (HESS J1841–055)

1. INTRODUCTION

In the last three years, the Large Area Telescope (LAT; Atwood et al. 2009) aboard the *Fermi* satellite has proven a revolutionary detector of gamma-ray pulsars¹⁵. These objects are rapidly rotating, highly magnetized neutron stars, whose rotation carries the gamma-ray emitting regions past an observer’s line of sight, creating periodic pulsations.

With the LAT, pulsars have been detected via three different approaches. First, for pulsars known from radio observations, gamma-ray pulsations are detected by coherent folding of the LAT photon arrival times based on the provided pulsar ephemerides (e.g., Abdo et al. 2010c; Guillemot et al.

2012). Second, radio searches of unassociated gamma-ray sources, as listed in the *Fermi*-LAT Second Source Catalog (2FGL; Nolan et al. 2012), have revealed new radio pulsars. The ephemerides obtained from radio timing observations are in turn used to coherently phase-fold the LAT data and probe for gamma-ray pulsations (e.g.; Ransom et al. 2011; Cognard et al. 2011; Camilo et al. 2011; Kerr et al. 2012; Ray et al. 2012).

Contrasting the previous two strategies, “blind searches” are not guided by prior knowledge of the pulsar parameters (see e.g. Chandler et al. 2001). Within a year after launch of *Fermi*, previous blind searches had impressively unveiled 24 pulsars (Abdo et al. 2009a; Saz Parkinson et al. 2010) using a time-differencing technique (Atwood et al. 2006; Ziegler et al. 2008). Another two pulsars were found after two years (Saz Parkinson et al. 2012), however the detection rate had dropped since then, predominantly because of the increasing computational challenge with the longer data time span.

The sensitivity of blind searches for gamma-ray pulsars is limited by computing cost, because a grid in the search parameter space (for isolated systems typically sky location, frequency f , and spin-down rate \dot{f}) must be explicitly searched. The number of grid points required to discretely cover the relevant parameter space increases as a high power of the coherent integration time (e.g., Brady et al. 1998). This problem is analogous to blind searches for continuous gravitational waves (CWs) emitted from rapidly spinning neutron stars, where hierarchical strategies (Schutz & Papa 2000; Brady & Creighton 2000; Krishnan et al. 2004; Cutler et al. 2005) and semi-coherent methods are used to efficiently scan wide parameter-space ranges in years of data at finite computational resources.

Here, we present the discovery and key parameters of a young, energetic gamma-ray pulsar, PSR J1838–0537, detected during a new blind survey exploiting a novel data-analysis method (Pletsch et al. 2012) originally developed to blindly search for weak CW signals (Pletsch & Allen 2009;

¹ Max-Planck-Institut für Gravitationsphysik (Albert-Einstein-Institut), 30167 Hannover, Germany

² Leibniz Universität Hannover, 30167 Hannover, Germany

³ email: holger.pletsch@aei.mpg.de

⁴ Max-Planck-Institut für Radioastronomie, Auf dem Hügel 69, 53121 Bonn, Germany

⁵ email: guillemo@mpifr-bonn.mpg.de

⁶ Department of Physics, University of Wisconsin-Milwaukee, P.O. Box 413, Milwaukee, WI 53201, USA

⁷ Jodrell Bank Centre for Astrophysics, School of Physics and Astronomy, The University of Manchester, M13 9PL, UK

⁸ Rice University, Department of Physics and Astronomy, MS-108, P. O. Box 1892, Houston, TX 77251, USA

⁹ Columbia Astrophysics Laboratory, Columbia University, New York, NY 10027, USA

¹⁰ INAF-Istituto di Astrofisica Spaziale e Fisica Cosmica, 20133 Milano, Italy

¹¹ Space Science Division, Naval Research Laboratory, Washington, DC 20375-5352, USA

¹² W. W. Hansen Experimental Physics Laboratory, Kavli Institute for Particle Astrophysics and Cosmology, Department of Physics and SLAC National Accelerator Laboratory, Stanford University, Stanford, CA 94305, USA

¹³ National Radio Astronomy Observatory (NRAO), Charlottesville, VA 22903, USA

¹⁴ Santa Cruz Institute for Particle Physics, Department of Physics and Department of Astronomy and Astrophysics, University of California at Santa Cruz, Santa Cruz, CA 95064, USA

¹⁵ See <https://confluence.slac.stanford.edu/display/GLAMCOG/Public+List+of+LAT-Detected+Gamma-Ray+Pulsars/>

Pletsch 2010, 2011). The pulsar is spatially coincident with the extended source HESS J1841–055 (Aharonian et al. 2008), detected at very high energies (VHE; $E > 0.1$ TeV). We show that the pulsar’s energetics make this association plausible.

2. DISCOVERY OF PSR J1838–0537

In recent work (Pletsch et al. 2012) we reported on the discovery of nine new gamma-ray pulsars in this novel, ongoing blind survey using 975 days of LAT data. Unlike those nine pulsars, PSR J1838–0537, being significantly younger, was initially detected only during the first year of data (before its large glitch). After the glitch, recovering the (weaker) pulsations proved to be a substantial challenge requiring a dedicated follow-up study presented below (Section 3).

In the new blind-search effort, detecting PSR J1838–0537, we have utilized a hierarchical (multistage) approach. The first stage is semi-coherent, where coherent Fourier powers computed over a 6-day window are incoherently combined by sliding the window over the entire 975 days of data. A fundamental new element of the search method is the exploitation of a parameter-space metric (Pletsch & Allen 2009; Pletsch 2010) to build an efficient search grid (in f , \dot{f} and sky position). In a second stage, significant semi-coherent candidates are automatically followed up via a fully coherent analysis. A third stage further refines coherent pulsar candidates by using higher signal harmonics adopting the H -test (de Jager et al. 1989). Further advances incorporated are described in Pletsch et al. (2012).

The survey targets unassociated sources from the 2FGL catalog with “pulsar-like” properties. Such sources feature significantly curved emission spectra and low flux variability over time. Further details on the survey regarding source selection, data preparation and search parameter-space are found in Pletsch et al. (2012).

We have detected PSR J1838–0537 as part of the survey in the blind search of 2FGL J1839.0–0539. This source also has gamma-ray counterparts 1FGL J1839.1–0543c in the *Fermi*-LAT First Source Catalog (Abdo et al. 2010a) and 0FGL J1839.0–0549 in the *Fermi* Bright Source List (Abdo et al. 2009b).

3. FOLLOW-UP ANALYSIS

3.1. Data Preparation

For the follow-up study, we prepared a dedicated LAT data set extending the blind-search input data to 1168 days, up to 2011 October 17. Using the *Fermi* Science Tools¹⁶, we selected LAT photons whose reconstructed directions lie within 15° of the pulsar, have energies above 100 MeV, and zenith angles $\leq 100^\circ$. We included only “Source”-class photons according to the P7_V6 Instrument Response Functions and excluded times when the satellite’s rocking angle exceeded 52° .

To improve the signal-to-noise ratio, each photon is assigned a weight measuring the probability that it has originated from the pulsar (Kerr 2011). These weights are computed through a binned likelihood analysis (as done for the original blind-search input data) using a spectral model for the region including all 2FGL-catalog sources found within 15° of PSR J1838–0537. The pulsar spectrum is modeled as an exponentially cutoff power law, $dN/dE \propto E^{-\Gamma} \exp(-E/E_c)$, where Γ is the photon index and E_c is the cutoff energy.

¹⁶ <http://fermi.gsfc.nasa.gov/ssc/data/analysis/scitools/overview.html>

TABLE 1
PARAMETERS OF PSR J1838–0537

Parameter	Value
Right ascension, α (J2000.0)	18 ^h 38 ^m 56 ^s .02(3)
Declination, δ (J2000.0)	−05°37′09″(2)
Galactic longitude, l (°)	26.5
Galactic latitude, b (°)	0.2
Spin frequency, f (Hz)	6.863015715(4) ^a
	6.86305339(1) ^b
Frequency 1st derivative, \dot{f} (10^{-11} Hz s ^{−1})	−2.18964(6) ^a
	−2.2222(1) ^b
Frequency 2nd derivative, \ddot{f} (10^{-22} Hz s ^{−2})	5.0(4) ^a
	17.0(9) ^b
Epoch (MJD)	55100.0
Data span (MJD)	54702 – 55836
Characteristic age, τ_c (yr)	4970
Spin-down power, \dot{E} (erg s ^{−1})	5.9×10^{36}
Surface magnetic field strength, B_S (G)	8.3×10^{12}
Light-cylinder magnetic field strength, B_{LC} (kG)	24.7
Photon index, Γ	1.8 ± 0.1
Cutoff energy, E_c (GeV)	5.6 ± 1.4
Photon flux above 100 MeV (10^{-8} photons cm ^{−2} s ^{−1})	23.9 ± 5.1
Energy flux above 100 MeV (10^{-11} erg cm ^{−2} s ^{−1})	17.5 ± 1.8

NOTE. — Numbers in parentheses are statistical 1σ errors in the last digits.

^a Pre-glitch solution (before MJD 55100).

^b Post-glitch solution (after MJD 55450).

The extragalactic diffuse emission and the residual background are modeled jointly using the *iso_p7v6source* template, and the Galactic diffuse emission is modeled using the *gal_2yearp7v6_v0* map cube. For computational feasibility, only the 165 000 photons with the highest weights are considered (implying a probability-weight threshold of 0.018).

3.2. Pulsar Timing and Glitch Analysis

Using the 1168-day data set, the initial pulsar parameters are further refined through a timing-analysis procedure. With techniques described in Ray et al. (2011), pulse Times Of Arrival (TOAs) are precisely measured and parameters of a timing model are fit to these measurements.

TOAs are obtained from subdividing the follow-up data set into 40 segments of about equal length. The initial pulsar parameters are used to fold the photon arrival times and produce a set of pulse profiles. By cross-correlating each pulse profile with a multi-Gaussian template derived from fitting the entire data set, the TOAs are determined using the unbinned-maximum-likelihood method of Ray et al. (2011). Then TEMPO2 (Hobbs et al. 2006) is used to fit the TOAs to a timing model including sky position, frequency and frequency derivatives.

As is typical for a youthful pulsar, PSR J1838–0537 shows irregularities in its spin-frequency evolution that are of two types: (i) timing noise, observed as slowly varying, non-deterministic fluctuations in frequency, which can be modeled by including a second frequency derivative in fitting the TOAs; (ii) glitch activity, an abrupt spin-frequency increase, typically followed by a recovery phase towards the pre-glitch rotational state. Thus, the glitch of PSR J1838–0537 leads to rapid loss of phase coherence in the timing analysis if not additionally accounted for.

The spin-parameter changes after the glitch are estimated in a dedicated analysis. Fixing the sky position at the pre-glitch (before MJD 55100) timing solution, ranges in frequency f ,

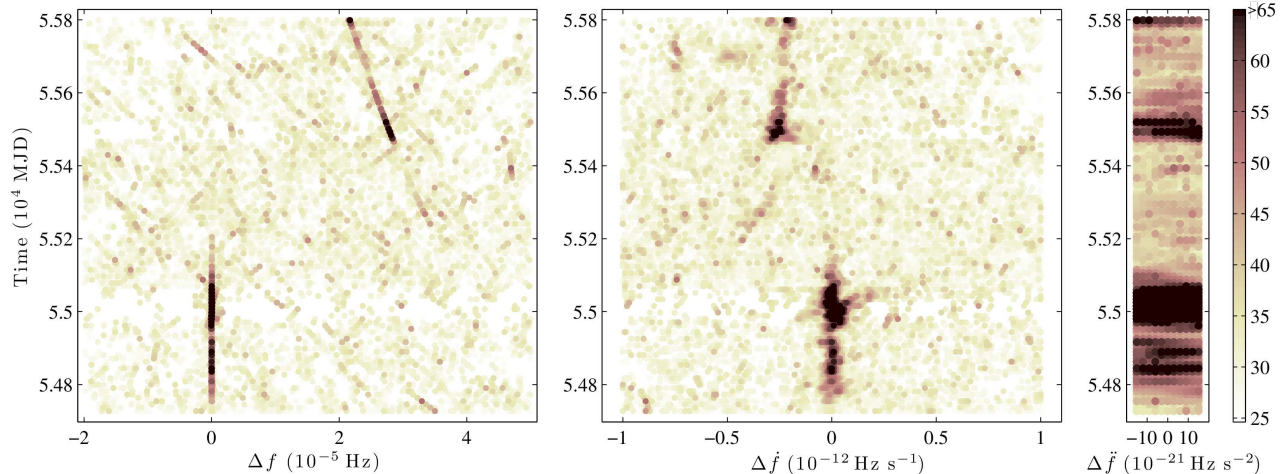


FIG. 1.— Pulsar glitch analysis. Color-coded is the weighted H -test statistic for photons lying within a 90-day window that is slid over the entire data set with 90% overlap. Fixing the sky position at the pre-glitch (before MJD 55100) solution, for each window scans in H -test over $\{f, \dot{f}, \ddot{f}\}$ are done. Vertical axes show the time midpoint of each window. Horizontal axes show the offsets from the inferred pre-glitch parameters in f (left), \dot{f} (middle), and \ddot{f} (right).

frequency derivative \dot{f} , and second frequency derivative \ddot{f} are scanned on a dense grid around their pre-glitch values, computing the weighted H -test (Kerr 2011) at each grid point using photons within a fixed time window. As a balance between signal-to-noise ratio and time resolution, we use a window size of 90 days, which is just long enough to still produce a detectable signal-to-noise ratio. This 90-day window is slid over the entire data set with 90% overlap between subsequent steps. The results (Figure 1) indicate that the pulsar experienced a glitch near MJD 55100. However, immediately after the nominal glitch epoch no convincing signal is detected for a period of about 300 days. This might be due to the pulsar’s frequency changing faster during early glitch recovery than the $\{f, \dot{f}, \ddot{f}\}$ phase model used. In this respect, shorter window sizes would possibly help, but these are prohibited by the sparse sampling of LAT photons.

From Figure 1, estimated values for the glitch parameters are added to the timing model, serving as input to iterate the above timing procedure. Table 1 shows the obtained phase-coherent timing solution. The measured post-glitch spin parameters imply a relative increase in f of $\Delta f/f \sim 5.5 \times 10^{-6}$ and a relative decrease in \dot{f} of $-\Delta \dot{f}/\dot{f} \sim 1.5\%$. In addition, the timing solution requires a relative increase in \ddot{f} of $\Delta \ddot{f}/\ddot{f} \sim 2.4$, which likely accounts mainly for timing noise. In terms of $\Delta f/f$, this glitch is in the top 5% of all pulsar glitches recorded to date (Espinoza et al. 2011), and is the largest observed for any gamma-ray-only pulsar (Dormody et al. 2012). Measuring such strong pulsar glitches is important, as they may allow probing the physics of neutron-star interiors (e.g., Shapiro & Teukolsky 1983; Haskell et al. 2012).

The measured parameters listed in Table 1 characterize the pulsar as young and energetic. The implied characteristic age and surface magnetic field strength are $\tau = -f/2\dot{f} = 4970$ yr and $B_S = 3.2 \times 10^{19} (-\dot{f}/f^3 \text{ s}^{-1})^{1/2} \text{ G} = 8.3 \times 10^{12} \text{ G}$. Assuming a neutron-star moment of inertia of $I = 10^{45} \text{ g cm}^2$, the pulsar’s spin-down power is derived as $\dot{E} = -4\pi^2 I f \dot{f} = 5.9 \times 10^{36} \text{ erg s}^{-1}$.

3.3. Pulse Profile and Spectral Parameters

Figure 2 shows the phase-time diagram and pulse profile using the timing solution of Table 1. In the integrated pulse

profile (weighted pulse phase histogram) statistical errors are obtained as $(\sum_j w_j^2)^{1/2}$, where j runs over all photons in the same phase bin and w_j denotes the j th photon’s probability weight. Comparing the gamma-ray emission before and after the glitch, we found no observable changes in flux, pulse profile or spectrum of the pulsar, consistent with other LAT-pulsar glitches (Dormody et al. 2012).

The integrated pulse profile of PSR J1838–0537 is fitted by two Lorentzian lines. The Full-Widths at Half Maxima (FWHM) for the first (P1) and second (P2) peak are 0.18 ± 0.09 and 0.13 ± 0.05 , respectively. The separation between the two is $\Delta = 0.24 \pm 0.04$. Figure 2 also exhibits a decrease in the ratio of peaks P1 and P2 with increasing energy. Also observed in other LAT pulsars (see e.g. Abdo et al. 2010c; Noutsos et al. 2011; Abdo et al. 2010d), this is thought to be caused by varying gamma-ray emission altitudes and curvature radii of the magnetic field lines as the pulsar rotates (Abdo et al. 2010d).

Observing pulsed emission out to $E_{\text{max}} \sim 10 \text{ GeV}$ implies transparency to magnetic pair creation. This bounds the altitude r of emission (e.g., Abdo et al. 2010b), giving $r \geq (E_{\text{max}} B_{12}/2.7 \text{ GeV})^{2/5} P^{-1/5} R_*$ in flat spacetime (Story & Baring, in preparation) for surface fields $10^{12} B_{12} \text{ G}$. For PSR J1838–0537 one obtains $r \gtrsim 6.1 R_*$, precluding emission near the stellar surface.

Table 1 lists the best-fit values for Γ , E_c , and the photon and energy fluxes of PSR J1838–0537 as derived from a spectral analysis of the region, restricted to photons with pulse phases between 0 and 0.5 maximizing the pulsar’s contribution. Further details on the spectral analysis of PSR J1838–0537 and a search for unpulsed gamma-ray emission from a putative pulsar wind nebula (PWN) in the off-pulse phase interval will be reported elsewhere (Aharonian et al. 2012).

3.4. Pulsation Significance

Over the 1168 days, the obtained timing solution yields a weighted H -test of 486.4, being extremely significant with a single-trial false alarm probability of $\sim 10^{-92}$ (Kerr 2011).

Figure 3 investigates how this H -test value accumulates over time. As expected, the signal increases linearly during times where the timing solution describes the pulsar’s rota-

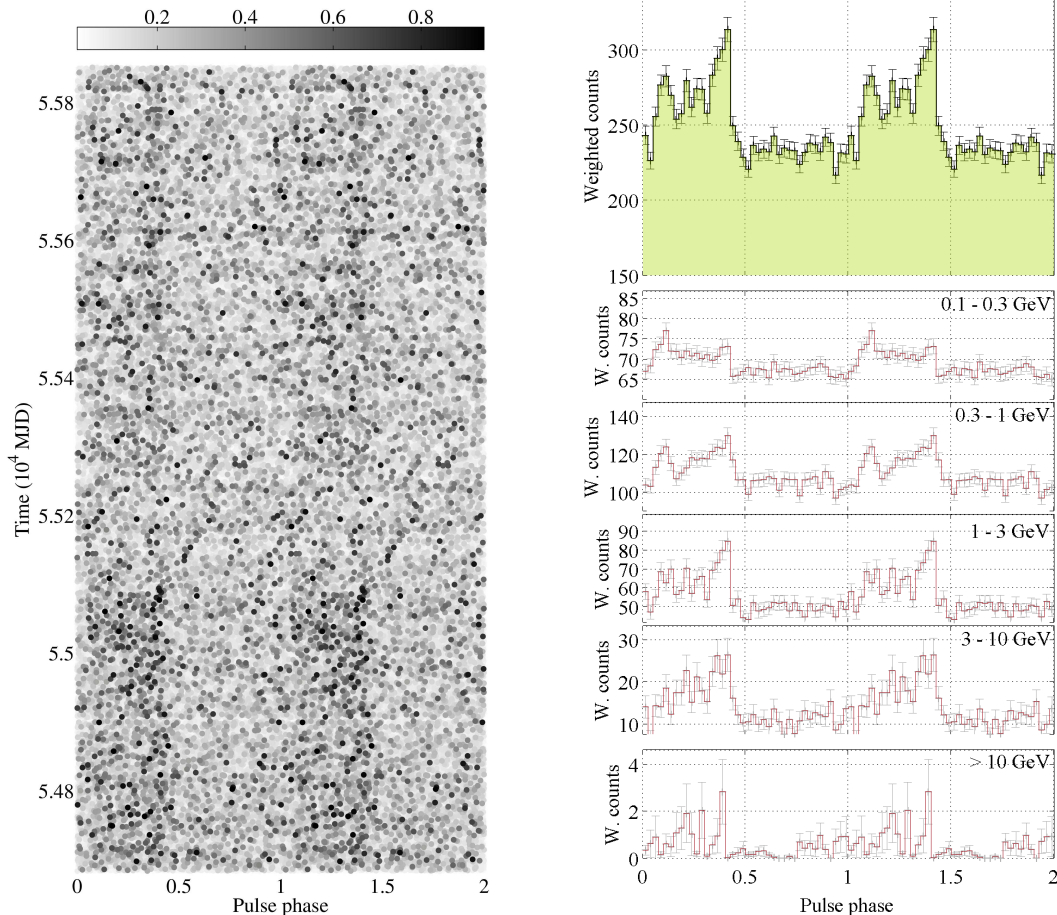


FIG. 2.— Left: Phase-time diagram, showing the pulse phase for each photon arrival time with the photon probability weight represented by gray-scale intensity. Right: The upper plot shows the integrated pulse profile (40 bins per rotation); error bars represent 1σ statistical uncertainties. The five plots below show integrated pulse profiles in different energy ranges. For clarity, horizontal axes always show two rotations.

tional behavior well (before the glitch at MJD 55100 and after MJD 55450). However, comparing the two different slopes from linear fits made during both time intervals, the slope during the post-glitch interval is smaller by about 27%.

This effect is traced back to a reduction in exposure resulting from a change in *Fermi*-LAT’s sky-survey observing pattern on 2009 September 3 (MJD 55077). This change has decreased the average exposure at the pulsar’s sky position by about 24% (Figure 3, middle panel). Hence, the exposure reduction explains (within 3%) the smaller rate in H -test increase over the later data (the H -test is linear in the number of photons). This is further confirmed by observing no significant variation in weighted photon flux over time (Figure 3, lower panel).

4. MULTIWAVELENGTH OBSERVATIONS

4.1. Radio and X-ray Counterpart Searches

To determine whether PSR J1838–0537 is also visible as a radio pulsar, a 1.7-hr observation has been conducted on 2011 May 27 with the Green Bank Telescope (GBT) at 2 GHz. We also analyzed a 1-hr archival GBT observation from on 2009 July 5 at 0.8 GHz (Ransom et al. 2011). Configuration details of both radio observations are found in Table 5 of Pletsch et al. (2012). Folding the data using the timing solution of Table 1 and only searching in dispersion measure revealed no radio pulsations.

As in Pletsch et al. (2012), upper limits on the radio flux density are derived with the modified radiometer equation (Lorimer & Kramer 2005). The sensitivity loss due to the telescope pointing-direction offset from the pulsar position ($0.5'$ and $5.7'$, respectively) is appropriately accounted for, analogously to Pletsch et al. (2012), leading to radio flux upper limits of $9 \mu\text{Jy}$ for the 2 GHz observation, and $82 \mu\text{Jy}$ for the 0.8 GHz observation. These upper limits are comparable with those obtained for other LAT-discovered pulsars (Ray et al. 2011; Pletsch et al. 2012) suggesting that PSR J1838–0537 is radio-quiet.

In searching for X-ray counterparts, two archival *Swift* observations (4.5 ks total exposure) cover the position of PSR J1838–0537, but no counterpart is observed. Using a 41.1-ks *Suzaku* observation, we find a hint of X-ray emission at the pulsar location. However, the *Suzaku* large positional uncertainty ($\sim 30''$) and the low confidence ($\sim 3\sigma$) of the counterpart candidate preclude a firm X-ray detection of the pulsar. The unabsorbed flux upper limit in the 0.3–10 keV energy range computed as in Marelli et al. (2011) is $5.0 \times 10^{-14} \text{ erg cm}^{-2} \text{ s}^{-1}$, similar to other LAT pulsars (Marelli et al. 2011; Pletsch et al. 2012).

4.2. A Likely Pulsar Wind Nebula Association

The sky position of PSR J1838–0537 coincides with the unidentified VHE source HESS J1841–055 discovered dur-

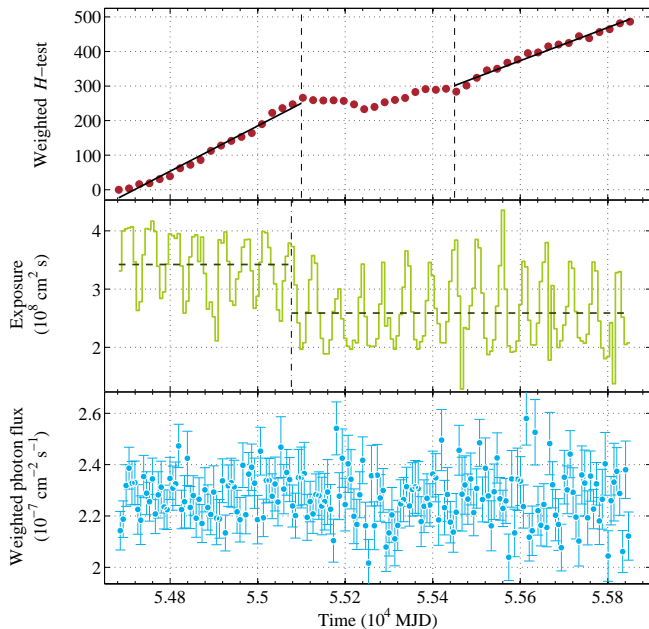


FIG. 3.— Upper panel: Weighted H -test statistic as a function of time using the timing solution of Table 1 (dotted curve). Black solid lines represent separate linear fits before the nominal glitch (before MJD 55100), and after recovery of pulsations (from MJD 55450) where the measured slope is smaller by 27%. Middle panel: Exposure for the pulsar’s sky location in time bins of size 6.7 days. The average exposure (horizontal dashed line) after the LAT’s observing-pattern change at MJD 55077 (vertical dashed-dotted line) is smaller by 24%. The exposure oscillation is at the 53.4-day precession period of the spacecraft orbit. Lower panel: Sum of photon probability weights per time bin divided by exposure. Binning in time is identical to the middle panel and error bars represent 1σ statistical uncertainties.

ing the H.E.S.S. Galactic Plane Survey (Aharonian et al. 2008). Although its extended TeV morphology suggests that HESS J1841–055 is composed of multiple sources, limited exposure has hitherto prohibited statistically significant confirmation. None of the previously known counterparts proposed in Aharonian et al. (2008) is capable of fully accounting for the VHE emission alone.

PSR J1838–0537 is sufficiently energetic to power a PWN, further supporting this association. With distance d to the pulsar, the spin-down flux at Earth is \dot{E}/d^2 . If assuming a pseudo-distance¹⁷ based on the observed correlation between the gamma-ray luminosity (0.1–100 GeV) and \dot{E} (following Saz Parkinson et al. 2010) of 2 kpc this yields a large spin-down flux $\dot{E}/d^2 \sim 1.5/d_{2\text{kpc}}^2 \times 10^{36} \text{ erg s}^{-1} \text{ kpc}^{-2}$ (where $d_{2\text{kpc}} = d/2 \text{ kpc}$), which is comparable to similar systems (Carrigan et al. 2008).

The integral energy flux of HESS J1841–055 at the detector over the range 0.5–80 TeV is $G_{\text{VHE}} \sim 5.8 \times 10^{-11} \text{ erg cm}^{-2} \text{ s}^{-1}$ (Sguera et al. 2009). Assuming isotropic emission this implies a conversion efficiency $\eta = L_{\gamma}/\dot{E} = 0.5 d_{2\text{kpc}}^2 \%$ (0.5–80 TeV), similar to other suggested pulsar/PWN associations (Hessels et al. 2008).

4.3. A Nearby Candidate Supernova Remnant

Because the pulsar is very young, we also consider the possible association with the nearby candidate supernova

remnant (SNR) G26.6–0.1. This diffuse X-ray source was detected in the ASCA Galactic Plane Survey (Bamba et al. 2003). The best-fit absorption column density of the X-ray spectrum Bamba et al. (2003) yields a distance estimate of 1.3 kpc.

The SNR candidate has an angular size of about $12'$ (FWHM), and its approximate geometric center lies $20'$ away from the pulsar’s sky position. We note that the probability of chance superposition is also not negligible (Kaspi 1998). To assess the SNR association, we assume the 1.3 kpc distance and an age of 5 kyr, and consider the corresponding pulsar transverse velocity obtained as $\sim 1500 (d/1.3 \text{ kpc}) \text{ km s}^{-1}$. This is about 50% faster than the highest velocity directly measured for a neutron star (Chatterjee et al. 2005). However, the distance is quite uncertain and could be significantly smaller, which would reduce the resulting transverse velocity. Thus the SNR association appears unlikely, but cannot be fully excluded.

5. CONCLUSIONS

We report the discovery and follow-up study of PSR J1838–0537 found in a new blind-search effort using *Fermi*-LAT data. The inferred parameters distinguish the pulsar as young and energetic. The characteristic age, $\tau = 4970 \text{ yr}$, makes PSR J1838–0537 the second-youngest pulsar ever found in a blind search of gamma-ray data, after PSR J1023–5746 (Saz Parkinson et al. 2010), for which $\tau = 4610 \text{ yr}$. Considering all rotation-powered pulsars known, PSR J1838–0537 resides among the top 1% of systems with largest \dot{E} . In deep radio observations no pulsations have been detected, suggesting that PSR J1838–0537 is radio-quiet, only detectable through its gamma-ray pulsations. Moreover, the pulsar experienced the largest glitch yet observed in any gamma-ray-only pulsar.

The pulsar’s sky location coincides with the extended VHE source HESS J1841–055. We have shown that the pulsar’s energetics are likely to power a PWN producing part of the H.E.S.S.-detected TeV emission. This clearly motivates a further analysis of the region at TeV energies to confirm such a PWN association. With the LAT, an analysis for off-pulse emission of PSR J1838–0537 will help studying a potential PWN and the ambient medium (e.g., Ackermann et al. 2011).

PSR J1838–0537, the tenth object found in this new survey, brings the number of gamma-ray pulsars undetected in radio to 33 (Ray et al. 2012). Together, these represent a significant increase of the gamma-ray-only pulsar population and will be an important contribution to the second *Fermi*-LAT Pulsar Catalog (Abdo et al. 2012). In addition to the improved search techniques (Pletsch et al. 2012), the computational resources for the survey have recently been significantly enhanced by using the volunteer computing system *Einstein@Home*¹⁸. The unprecedented search sensitivity from the combination of these advances warrants optimism for further gamma-ray pulsar discoveries.

We thank M.-H. Grondin, M. Lemoine-Goumard and J. Méhault for helpful discussions on HESS J1841–055. This work was partly supported by the Max-Planck-Gesellschaft and by U.S. National Science Foundation Grants 0970074 and 1104902. The *Fermi* LAT Collaboration acknowledges support from several agencies and institutes for both development

¹⁷ This pseudo-distance is subject to various caveats that translate to considerable uncertainties in this estimate of factors of a few (Saz Parkinson et al. 2010).

¹⁸ <http://einstein.phys.uwm.edu/>

and the operation of the LAT as well as scientific data analysis. These include NASA and DOE in the United States, CEA/Irfu and IN2P3/CNRS in France, ASI and INFN in Italy, MEXT, KEK, and JAXA in Japan, and the K. A. Wallenberg

Foundation, the Swedish Research Council and the National Space Board in Sweden. Additional support from INAF in Italy and CNES in France for science analysis during the operations phase is also gratefully acknowledged.

REFERENCES

- Abdo, A. A., et al. 2009a, *Science*, 325, 840
 Abdo, A. A., et al. 2009b, *ApJS*, 183, 46
 Abdo, A. A., et al. 2010a, *ApJS*, 188, 405
 Abdo, A. A., et al. 2010b, *ApJ*, 708, 1254
 Abdo, A. A., et al. 2010c, *ApJS*, 187, 460
 Abdo, A. A., et al. 2010d, *ApJ*, 713, 154
 Abdo, A. A., et al. 2012, in preparation
 Ackermann, M., et al. 2011, *ApJ*, 726, 35
 Aharonian, F., et al. 2008, *A&A*, 477, 353
 Aharonian, F., et al. 2012, in preparation
 Atwood, W. B., Ziegler, M., Johnson, R. P., & Baughman, B. M. 2006, *ApJ*, 652, L49
 Atwood, W. B., et al. 2009, *ApJ*, 697, 1071
 Bamba, A., Ueno, M., Koyama, K., & Yamauchi, S. 2003, *ApJ*, 589, 253
 Brady, P. R., & Creighton, T. 2000, *Phys. Rev. D*, 61, 082001
 Brady, P. R., Creighton, T., Cutler, C., & Schutz, B. F. 1998, *Phys. Rev. D*, 57, 2101
 Camilo, F., et al. 2011, *ApJ*, 746, 39
 Carrigan, S., Hinton, J. A., Hofmann, W., & et al. 2008, in *Proc. 30th Int. Cosmic Ray Conf.*, ed. R. Caballero et al., Vol. 2, 659
 Chandler, A. M., et al. 2001, *ApJ*, 556, 59
 Chatterjee, S., et al. 2005, *ApJ*, 630, L61
 Cognard, I., et al. 2011, *ApJ*, 732, 47
 Cutler, C., Gholami, I., & Krishnan, B. 2005, *Phys. Rev. D*, 72, 042004
 de Jager, O. C., Raubenheimer, B. C., & Swanepoel, J. W. H. 1989, *A&A*, 221, 180
 Dormody, M., et al. 2012, in preparation
 Espinoza, C. M., Lyne, A. G., Stappers, B. W., & Kramer, M. 2011, *MNRAS*, 414, 1679
 Guillemot, L., et al. 2012, *ApJ*, 744, 33
 Haskell, B., Pizzochero, P. M., & Sidery, T. 2012, *MNRAS*, 420, 658
 Hessels, J. W. T., et al. 2008, *ApJ*, 682, L41
 Hobbs, G. B., Edwards, R. T., & Manchester, R. N. 2006, *MNRAS*, 369, 655
 Kaspi, V. M. 1998, *Adv. Space Res.*, 21, 167
 Kerr, M. 2011, *ApJ*, 732, 38
 Kerr, M., et al. 2012, *ApJ*, 748, L2
 Krishnan, B., et al. 2004, *Phys. Rev. D*, 70, 082001
 Lorimer, D. R., & Kramer, M. 2005, *Handbook of Pulsar Astronomy* (Cambridge: Cambridge Univ. Press)
 Marelli, M., De Luca, A., & Caraveo, P. A. 2011, *ApJ*, 733, 82
 Nolan, P. L., et al. 2012, *ApJS*, 199, 31
 Noutsos, A., et al. 2011, *ApJ*, 728, 77
 Pletsch, H. J. 2010, *Phys. Rev. D*, 82, 042002
 Pletsch, H. J. 2011, *Phys. Rev. D*, 83, 122003
 Pletsch, H. J., & Allen, B. 2009, *Phys. Rev. Lett.*, 103, 181102
 Pletsch, H. J., et al. 2012, *ApJ*, 744, 105
 Ransom, S. M., et al. 2011, *ApJ*, 727, L16
 Ray, P. S., et al. 2011, *ApJS*, 194, 17
 Ray, P. S., et al. 2012, arXiv:1205.3089
 Saz Parkinson, P. M., et al. 2010, *ApJ*, 725, 571
 Saz Parkinson, P. M., et al. 2012, in preparation
 Schutz, B. F., & Papa, M. A. 2000, in *Proc. Moriond Meeting on Gravitational Waves and Experimental Gravity*, ed. J. T. T. Van, J. Dumarchez, S. Raynoud, C. Salomon, S. Thorsett, & J. Y. Vinet (Hanoi, Vietnam: World Publishers), 199
 Sguera, V., et al. 2009, *ApJ*, 697, 1194
 Shapiro, S. L., & Teukolsky, S. A. 1983, *Black Holes, White Dwarfs and Neutron Stars. The Physics of Compact Objects* (New York: Wiley-Interscience)
 Ziegler, M., Baughman, B. M., Johnson, R. P., & Atwood, W. B. 2008, *ApJ*, 680, 620